Mon. Not. R. Astron. Soc. **000**, 1–?? (2014) Printed 3 February 2015 (MN LaTeX style file v2.2)

arXiv:1502.00017v1 [astro-ph.GA] 30 Jan 2015

Stellar feedback from high-mass X-ray binaries in cosmological hydrodynamical simulations

M. C. Artale[1]⋆ , P. B. Tissera[1,2,3] & L. J. Pellizza[4]
[1] *Instituto de Astronomía y Física del Espacio (IAFE, CONICET-UBA), C.C. 67 Suc. 28, C1428ZAA Ciudad de Buenos Aires, Argentina.*
[2] *Departamento de Ciencias Fisicas, Universidad Andres Bello, Av. Republica 220, Santiago, Chile.*
[3] *Millennium Institute of Astrophysics, Av. Republica 220, Santiago, Chile.*
[4] *Instituto Argentino de Radioastronomía, CONICET, Camino Gral. Belgrano km 40, Berazategui, Prov. de Buenos Aires, Argentina*

3 February 2015

ABSTRACT

We explored the role of X-ray binaries composed by a black hole and a massive stellar companion (BHXs) as sources of kinetic feedback by using hydrodynamical cosmological simulations. Following previous results, our BHX model selects low metal-poor stars ($Z = [0, 10^{-4}]$) as possible progenitors. The model that better reproduces observations assumes that a $\sim 20\%$ fraction of low-metallicity black holes are in binary systems which produce BHXs. These sources are estimated to deposit $\sim 10^{52}$ erg of kinetic energy per event. With these parameters and in the simulated volume, we find that the energy injected by BHXs represents $\sim 30\%$ of the total energy released by SNII and BHX events at redshift $z \sim 7$ and then decreases rapidly as baryons get chemically enriched. Haloes with virial masses smaller than $\sim 10^{10}\,M_{\odot}$ (or $T_{\rm vir} \lesssim 10^5$ K) are the most directly affected ones by BHX feedback. These haloes host galaxies with stellar masses in the range $10^7 - 10^8$ M$_{\odot}$. Our results show that BHX feedback is able to keep the interstellar medium warm, without removing a significant gas fraction, in agreement with previous analytical calculations. Consequently, the stellar-to-dark matter mass ratio is better reproduced at high redshift. Our model also predicts a stronger evolution of the number of galaxies as a function of the stellar mass with redshift when BHX feedback is considered. These findings support previous claims that the BHXs could be an effective source of feedback in early stages of galaxy evolution.

Key words: X-ray: binaries – galaxies: abundances, evolution

1 INTRODUCTION

The regulation of star formation activity (SF) in galaxies of different masses is still an open problem in cosmological simulations. Different feedback mechanisms have been proposed to regulate the transformation of gas into stars. Among them, supernova (SN) feedback is considered to play a critical role in the regulation of SF, with a larger impact for galaxies with circular velocities lower than $\sim 100\,{\rm km\,s^{-1}}$ (Dekel & Silk 1986). The SN feedback modelling in hydrodynamical codes has certainly helped to reach better agreement of the properties of the simulated galaxies with observations (e.g. Governato et al. 2007; Springel et al. 2006; Scannapieco et al. 2006). However, these studies also show that SN feedback might not be efficient enough to regulate the SF activity in low-mass systems, principally at high redshift. This problem manifests itself, for example, in the apparent inconsistency between the stellar-to-virial mass relation obtained from abundance matching techniques and that of hydrodynamical simulations in the low-mass end (e.g. Sawala et al. 2011; Moster et al. 2013; Behroozi et al. 2013). Different feedback mechanisms such as cosmic rays, radiative feedback or photoionization, among others, have been explored with the aim of improving the regulation of the SF in numerical models (e.g. Wadepuhl & Springel 2011; Stinson et al. 2012; Hopkins et al. 2014; Ceverino et al. 2014). However, much work is still needed to both understand the physical processes which regulate star formation as a function of redshift and to improve their modelling in numerical simulations.

High-mass X-ray binaries (HMXBs) are accretion-powered stellar systems composed by a black hole or a neutron star and a companion massive star, which emit X rays at typical luminosities of $10^{38}\,{\rm erg\,s^{-1}}$ (see Fabbiano 2006, for a review) and hence provide a radiative feedback on the interstellar medium. In some cases, they also produce

---

⋆ E-mail: mcartale@iafe.uba.ar

© 2014 RAS

collimated outflows (jets) with similar kinetic luminosities. These jets act as another feedback mechanism, heating the surrounding medium. The interest on HMBXs has increased in the last years because theoretical and observational works suggest that the production, and possibly the luminosity of these sources, could increase with decreasing metallicity of the stellar progenitor (e.g. Dray 2006; Linden et al. 2010; Kaaret et al. 2011; Brorby et al. 2014). Under this hypothesis, HMBXs could play an important role in the formation and evolution of galaxies at early epochs of the Universe.

Given their radiative feedback, HMXBs have been proposed as effective sources of reionization of the intergalactic medium (IGM) and of heating of the gas component in the small haloes in the very early Universe (e.g. Power et al. 2009). A recent report from Fragos et al. (2013) use the results of combining semi-analytical models of galaxy formation with a population synthesis code (Fragos et al. 2013), to compare the X-ray luminosity density produced by HMXBs and active galactic nuclei as a function of redshift, claiming that the first prevails at $z \gtrsim 6-8$. Different works have also studied the role of these binaries in the heating of the IGM and the shaping of the 21 cm signal from first galaxies (Power et al. 2013; Kaaret 2014; Fialkov et al. 2014; Pacucci et al. 2014). HMXBs have also been investigated as a source of reionization. Mirabel et al. (2011) suggest that the rate of ionizing photons emitted by HMXBs with black holes might be greater than that of their progenitor stars, and that these sources could heat the IGM up to 10^4 K, keeping it ionized. Using zoomed hydrodynamical simulations of mini-haloes, Jeon et al. (2014) have analysed the feedback from Population III (hereafter Pop III) HMXBs. Their results suggest that X-ray photons from these sources may suppress small scale structures and reduce the recombination rate in the IGM, providing a net positive feedback on reionization. Knevitt et al. (2014) investigated the effect of HMXBs on the high redshift IGM using a one-dimensional radiative transfer code. Contrary to previous works, they found that HMXBs do not produce neither any significant additional ionization nor heating of the IGM, except for the distant IGM in the case of continuous star formation. As it can be seen from the above discussion, the issue of the effects of the radiative feedback from HMXBs is far from being settled.

Recently, Justham & Schawinski (2012) studied high-mass X-ray binaries (HMXBs) as a potential source of feedback through the kinetic energy of their jets. Those HMXBs comprising black holes (hereafter, BHXs) are among the most powerful X-rays and jet emitters. The potential of BHXs as an efficient feedback mechanism at high redshift is supported by observational results from Fender et al. (2005) which suggest that the contribution of kinetic energy from BHX jets could be significant compared with the energy injected by SN, in some cases. Ramsey et al. (2006) studied the interstellar environment of seven HMXBs, showing that to understand the ionization and kinematics of the supershells around these sources, it is necessary that HMXBs contribute with a significant amount of kinetic energy. Several works indicate that the energy deposited by BHXs in the form of kinetic energy could be as high as their bolometric X-ray luminosities (Gallo et al. 2005; Pakull et al. 2010; Feng & Soria 2011; Soria et al. 2014). Based on these observational evidences, Justham & Schawinski (2012) conclude that the early injection of energy by these sources could heat up the ambient gas without expelling it from the galaxy, preventing the early transformation of gas into stars, and changing the properties of the ISM where SN events will take place. As we mentioned before, the main impact of this process is expected to occur at high redshift, where low-metallicity sources prevail.

In this paper, we implement for the first time, a BHX feedback model within cosmological hydrodynamical simulation, in a self-consistent way. Our simulations include a chemical evolution model (Scannapieco et al. 2005) and a physically-motivated SN feedback (Scannapieco et al. 2006), therefore the enrichment of baryons can be followed as galaxies are assembled. Hence, our simulations allows us to describe the metallicity dependence of the sources along the Hubble time. This gives us a further insight into this problem, by providing the self-consistent evolution of the gas cooling, the transformation of gas into stars and the stellar evolution, with the subsequent chemical enrichment of the baryons. We will consider very low-metallicity stars as BHX progenitors, since they are expected to be most energetic and abundant. We explore the effect of BHX feedback on the cosmic star formation history and on the properties of galaxies within haloes of different masses. Our results are in agreement to those reported by Justham & Schawinski (2012) where a semi-analytical model is developed to study the effects of BHX feedback.

This paper is summarized as follows. In Sect. 2 we describe the numerical simulations and the implementation of BHX feedback. In Sect. 3 we explore the effects of this feedback on the cosmic star formation history, while in Sect. 4 we study its effect on simulated galaxies. Finally, we present our main conclusions in Sect. 5.

2 NUMERICAL METHODOLOGY

In this section, we describe the main characteristics of the cosmological code, the simulations, and the model developed to incorporate the BHXs self-consistently in the numerical code.

2.1 The cosmological code

We use an extended version of the TreePM/SPH code P-GADGET-3 (Springel 2005), which includes a multiphase model for the gas component, metal-dependent cooling and SN feedback as described by Scannapieco et al. (2005, 2006).

The multiphase scheme allows the coexistence of low- and high-density gas clouds, diminishing the problems of over-smoothing of standard SPH. The main difference is that neighbouring particles are selected not only by a distance criterion, but also by considering their relative entropy. The decisions are made on a particle-particle basis, which implies no mass-dependent parameters to be fixed (see Scannapieco et al. 2006, for details). The multiphase model works coherently with the SN feedback model, which includes Type II and Type Ia SN events (hereafter, SNII and SNIa, respectively). When SN events are produced, metals and energy are distributed within the hot and cold gaseous phases surrounding the star particle representing a single stellar population. The cold phase of the star particle is defined by gas particles with $T < 2T_*$ and $\rho > 0.1\rho_*$, while the rest of the gas determines the hot phase ($\rho_* = 7\times10^{-26}\,\mathrm{g\,cm^{-3}}$ and $T_* = 4\times10^4$ K, see Scannapieco et al. 2006 for a detailed discussion on these parameters). The fraction of energy distributed into the cold phase is defined by the parameter ϵ_c. An exploration of this parameter and its effects is given by Scannapieco et al. (2006, 2008). Here, we adopt $\epsilon_\mathrm{c} = 0.5$ as it has been done in previous works which used this SN feedback model (Scannapieco et al. 2009; De Rossi et al. 2013; Pedrosa et al. 2014). Note that these cold and hot gaseous phases are defined for the stellar populations where SN events are estimated to be produced, and for the only purpose of distributing metals and energy. They have no direct relation with the SPH integration itself. Hot gas particles thermalize immediately the SN energy they receive, whereas cold gas particles build up an energy reservoir. The feedback energy is stored in these reservoirs until gas particles have enough energy to change their entropy in order to match that of their surrounding hot neighbour media. When this occurs, the reservoir energy is pumped into the internal energy. This SN scheme is able to produce powerful, mass-loaded galactic winds as has been shown in previous works (e.g. Scannapieco et al. 2008, 2009).

Stars more massive than $8M_\odot$ are considered as SNII progenitors. We estimate the number of SNII by adopting the Initial Mass Function (IMF) of Chabrier (2003). For SNIa, we use the simple model of Mosconi et al. (2001) where the SNIa rate is estimated by adopting an observationally motivated ratio (~ 0.0015). The lifetimes of SNIa progenitors are randomly selected within the range [0.1–1] Gyr. This model, albeit simple, allows a good representation of the chemical patterns of the stellar populations (Jimenez et al. 2014). The initial chemical composition of the gas component is assumed to be primordial ($X_\mathrm{H} = 0.76$, $X_\mathrm{He} = 0.24$). The chemical model follows the enrichment by twelve isotopes: ^{1}H, ^{2}He, ^{12}C, ^{16}O, ^{24}Mg, ^{28}Si, ^{56}Fe, ^{14}N, ^{20}Ne, ^{32}S, ^{40}Ca and ^{62}Zn. For SNIa we adopt the nucleosynthesis model of Iwamoto et al. (1999) and for SNII that of Woosley & Weaver (1995). Chemical elements are distributed in a similar fashion as the energy, although 80% of the new elements are dumped into the cold phase (i.e. 20% goes into the hot phase). The cooling functions are metal-dependent (Sutherland & Dopita 1993).

2.1.1 Numerical experiments

The simulated volumes represent 14 Mpc comoving-side boxes, and are consistent with the cosmology Λ-CDM with $\Omega_\Lambda = 0.7$, $\Omega_\mathrm{m} = 0.3$, $\Omega_\mathrm{b} = 0.04$, $\sigma_8 = 0.9$, and $H_0 = 100h\ \mathrm{Mpc^{-1}\ km\,s^{-1}}$ with $h = 0.7$. Although this is not the current favourite set of cosmological parameters, we use it because it allow us to compare these simulations with previous ones. The variation of the cosmological parameters will not affect the conclusions of this work, which is related to the effects of feedback on the properties of the ISM and the regulation of star formation within individual galaxies. For this purpose, we compare runs of the same initial conditions but with different feedback mechanisms.

Initially, the simulations contain 230^3 dark matter particles and 230^3 gas particles (we will refer to these simulations as S230). The dark matter and initial gas particle masses are $\sim 9.1\times10^6\ M_\odot$ and $\sim 1.3\times10^6\ M_\odot$. The adopted gravitational softening length is 1.24 h^{-1} kpc. S230 runs were followed down to $z = 0$, but we focus the analysis on $z > 4$.

Higher numerical resolution runs of 2×320^3 particles were also performed to investigate the dependence on mass resolution (we will refer to these simulations as S320). The dark matter and initial gas mass in this case are $\sim 3.1\times10^6\ M_\odot$ and $\sim 4.9\times10^5\ M_\odot$, and the gravitational softening length is $0.5h^{-1}$ kpc. These simulations were run down to $z \sim 7$ due to their high computational cost. We adopted the same star formation and feedback parameters used in S230. As a consequence, the star formation activity starts at higher redshift since smaller systems are better resolved. As a result, the impact of BHXs occurs also at higher redshift in S320 than in S230. Nevertheless, this behaviour does not affect our analysis since we are always comparing runs with and without BHX feedback with the same resolution to draw conclusions.

We have run the same initial condition with SN feedback (S230-SN and S320-SN) and with SN+BHX feedback (S230-BHX and S320-BHX) in order to assess the effects clearly. Although in this work, we only discuss the most successful implementation, we have run the same initial conditions varying the parameters of the BHX models, as explained in the following section.

2.2 The stellar feedback model for BH-HMXBs

We are interested in studying the effects of the kinematic feedback of BHXs originated from very low-metallicity progenitors. As these metal-poor progenitors are expected to form principally in the Early Universe, their contribution should be relevant for the regulation of the star formation in the early stages of galaxy evolution. As mentioned in the Introduction, we considered previous results from Power et al. (2009) and Justham & Schawinski (2012) to develop our model, which is fully implemented within our SPH code.

We will consider BHX populations rather than individual sources due to the numerical resolution of our simulations. We assume that massive stars with metallicities in the range $Z_\mathrm{EMP} = [0, 10^{-4})$ will give origin to *extremely metal-poor* progenitors of BHXs (see below for more details). This metallicity range is taken as indicative, since there is no clear theoretical or observational value to be used. Nevertheless, theoretical works predict larger formation rates for $Z < 0.01Z_\odot$ (e.g. Linden et al. 2010). The upper limit represents the characteristic value of the oldest Population II stars (Belczynski et al. 2004). We would like to stress that although the upper metallicity limit was selected with this criterion, sensitive variations should not affect strongly our results. Note also that we are not modelling Pop III stars. We assume our sources to be very low metallicity stars but not representative of the first stars. Pop III sources are beyond the scope of this paper and would demand the treatment of other physical mechanisms which are not included in our code (e.g. Chen et al. 2014). Our model includes the $Z = 0$ stellar populations since there are not efficient mixing processes within the SPH kernel. Their treatment should increase the metallicity floor quickly from $Z = 0$.

In order to estimate the number of BHs produced in each young stellar population, we adopt the model of Georgy et al. (2009) for the evolution of massive stars. This model includes stellar rotation and a dependence of the type of compact remnant on the metallicity of the progenitor. The fraction of massive stars that end their life as BHs increases with decreasing metallicity. Therefore, for each young stellar population we estimate the number of BHs produced by adopting the IMF of Chabrier (2003). We consider stellar masses in the range of $30-120M_{\odot}$ and metallicities consistent with the defined $Z_{\rm EMP}$ interval. We assume that $\sim 20\%$ of low-metallicity BHs will end up in binary systems, producing a BHX ($f^{\rm EMP}_{\rm BHX}=0.20$). This value is roughly comparable to the 30 % reported by Power et al. (2009), after correcting by the different IMF adopted.

As we mentioned before, in BHXs the BH accretes mass from its companion star releasing a significant amount of energy in the form of radiation and outflows. Observational evidence from shock-ionized bubbles in the environment of these sources ($\sim$ 50–300 pc) suggests that their mechanical output energy would be around $\sim 10^{52}$ erg (Soria et al. 2014). On the other hand, many authors have reported that the kinetical power from accreting black holes could be as high as their Eddington luminosity limit (Pakull & Mirioni 2003; Pakull et al. 2010). For example, for Cygnus X-1 Gallo et al. (2005) have found that its jet transforms its total power into kinetic energy, and that the latter could be greater than its bolometric X-ray luminosity. Similar results have been found by Soria et al. (2010) for the microquasar S26 in NGC 7793, and by Soria et al. (2014) for an accreting BH in M83.

Motivated by these observations, we assume that the energy deposited by low-metallicity BHXs in the form of kinetic energy is $E_{\rm BHX}=10^{52}$ erg (Mirabel et al. 2011; Feng & Soria 2011). Assuming that a similar amount of energy is radiated in the X-ray band during ~ 3 Myr, the mean X-ray luminosity per source is $L_{\rm X,source}\sim 10^{38}\,{\rm erg\,s^{-1}}$, which is typical of HMXBs. We also tested larger and smaller energy values. Energies of the order of $E_{\rm BHX}=10^{53}$ erg sweep the gas in haloes too efficiently while lower values ($E_{\rm BHX}\sim 10^{51}$ erg) produce no significant impact on the regulation of the star formation activity.

Hence, for each young stellar population with metallicity in the range $Z_{\rm EMP}=[0,10^{-4})$, we estimate the number of BHXs as $N_{\rm BHX}=f^{\rm EMP}_{\rm BHX}\times N_{\rm BH}(Z)$ where $N_{\rm BH}(Z)$ is the number of BHs produced according to Georgy et al. (2009) and $f^{\rm EMP}_{\rm BHX}=0.20$, as we discussed before. Each of these $N_{\rm BHX}$ sources releases $E_{\rm BHX}=10^{52}$ erg into the ISM. We assume that this energy will be efficiently thermalized by the surrounding gas clouds where the the events took place. This hypothesis is supported by observational evidences that show that these events are expected to affect the region surrounding the stellar progenitors ($\sim$ 300 pc, e.g. Pakull et al. 2010). As a consequence, the released energy is dumped into the internal energy of the nearby cold gas phase, contributing to build up their energy reservoir.

3 THE COSMIC STAR FORMATION RATE DENSITY

The SN and BHX feedback mechanisms modify the thermodynamical properties of the ISM, thus affecting the transformation of gas into stars, which is the main effect we analyse in this paper. In order to have a global picture of their impact, we estimate the cosmic star formation rate density (cSFR) for both simulations, S230-SN and S230-BHX. As shown in Fig. 1, the confrontation of the cSFR with observational results compiled by Behroozi et al. (2013) suggests that the treatment of BHX feedback worked in the expected way, yielding an improved description of the observations. The factor $f^{\rm EMP}_{\rm BHX}\sim 0.20$ was actually chosen to be able to represent this observational relation[1]. However, this factor might vary if the $E_{\rm BHX}$ is changed accordingly so that the total amount of released energy per population remains within the same values. Otherwise, the effects on the ISM are found to be too weak or too strong. The fact that it agrees roughly with that derived by Power et al. (2009) is encouraging.

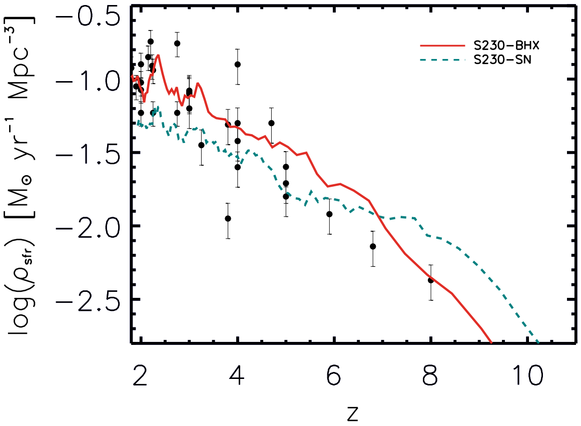

Figure 1. The cosmic star formation rate density estimated from simulations with SN feedback (S230-SN, blue dashed line) and with both SN and BHX feedbacks (S230-BHX, red solid line). For comparison, the observations compiled by Behroozi et al. (2013) are also included (black filled circles). The two runs share the same cosmology, and the SF and SN feedback parameters. The cosmic SFR is diminished by BHX feedback at early epochs ($z\gtrsim 7$) through cold gas heating, and boosted at lower redshift as more gas is available to feed the star formation activity.

In order to understand the combined effects of the two feedback mechanisms, in Fig. 2 (upper panel), we show the comoving energy density (e) released by SNII and BHXs, as a function of redshift, for both S230-SN and S230-BHX. We only considered SNII contributions since they also originate from massive stars. SNIa events will also contribute but with a larger time-scale and lower rate.

Both the SNII and the BHX energy contributions grow with redshift, due to the increasing cosmic star formation activity. However, BHX energy feedback grows at a slower rate than SNII one, due to the metallicity dependence of the progenitors. As the metallicity of the ISM increases, the number of BHX events diminishes, making SNe the dominating feedback mechanism. As can be seen from Fig. 2, BHX feedback is significant for $z>7$. As an example, at $z\gtrsim 7$ it represents $\sim 30\%$ of the total energy (SNII+BHX) released into the ISM. For lower redshift, the contribution

---

[1] For the adopted $E_{\rm BHX}=10^{52}$ erg, we tested $f^{\rm EMP}_{\rm BHX}$ between $\sim 1\%$ and $\sim 20\%$, finding $f^{\rm EMP}_{\rm BHX}\sim 0.20$ reproduced the observed trend (Fig. 1).

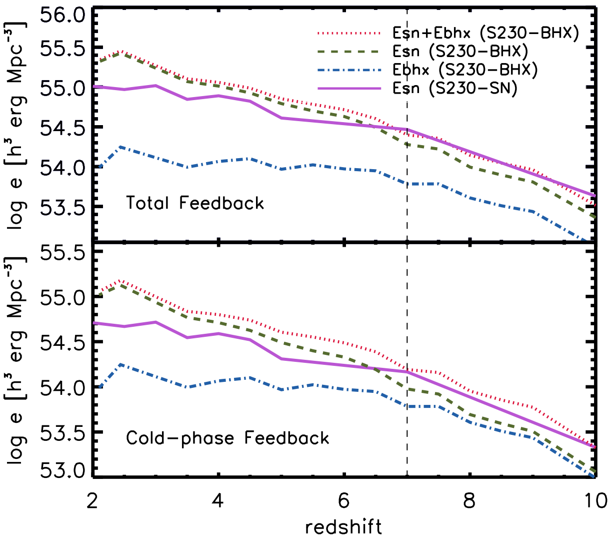

Figure 2. *Upper panel:* Comoving energy density released by different feedback mechanisms as a function of redshift: SNII in S230-SN (magenta solid line), SNII in SN230-BHX (green dashed line), and BHXs in S230-BHX (blue dot-dashed line). The total comoving energy density released by all agents in S230-BHXs (BHXs + SNe) is also plotted (red dotted line). BHXs release a significant amount of energy, of ∼30% of the SNII+BHX feedback at $z \gtrsim 7$, but its fractional contribution decays for lower redshifts, down to ∼10% at $z \sim 4$. *Lower panel:* Same as above, but taking into account only the energy injected into the cold gas phase of the ISM. The contribution of BHXs is larger in this case because they dump all their energy into the cold phase.

of BHX feedback progressively decays, reaching less than $\sim 10\%$ of the total at $z \sim 4$ ($\sim 5\%$ at $z \sim 2$). The total e released by SNII and BHX together is comparable to that of S230-SN for $z \gtrsim 7$, while for lower redshift, that of S230-BXH is greater due to the SFR enhancement triggered in this simulation, as can be seen in Fig. 1[2]. We will come back to this point later on.

The SNII and BHX energy release should affect the regulation of the star formation in different ways, depending on the energy available to heat up the cold gas clumps where stars are born. Fig. 2 (lower panel) displays the energy released by SNII and BHXs to the cold gas phase, as a function of redshift. For S230-BHX, the amount of energy dumped by BXHs at high redshift is similar to that of SNII. The total amount of feedback into the cold gas is then larger in S230-BHX than in S230-SN, producing an early heating of the gas that diminishes the star formation activity. In fact, this can be appreciated from the cSFR, shown in Fig. 1 for both simulations. As expected, in S230-BHX the BHX feedback diminishes the star formation activity for $z \gtrsim 7$ with respect to that of S230-SN, because it provides a larger amount of energy used directly in cold gas heating. The lower star formation rate in S230-BHX also explains the lower SNII feedback in this simulation (Fig. 2). We note that the star formation activity in S230-BHX increases for $z < 7$ faster than in S230-SN, reaching values comparable to observations (Behroozi et al. 2013). Hence, the impact of BHXs on the regulation of the star formation is boosted to lower redshift by making gas available to star formation at late times.

4 THE EFFECTS OF BHX FEEDBACK ON SIMULATED GALAXIES

In order to assess the effects of BHX feedback on the regulation of the star formation in galaxies of different masses, we first constructed galaxy catalogues from S230-SN and S230-BHX. We use the Friends-of-Friends technique to select the virialized structures, and the SUBFIND algorithm (Springel et al. 2001) to identify the substructures within the virial radii. We only consider simulated galaxies resolved with more than 500 particles. In order to test the robustness of our results against numerical resolution, we run a higher numerical resolution initial condition increasing the mass resolution by a factor of eight. We acknowledge the fact that our simulated volume is small to provide a complete description of the galaxy populations. However, by comparing the same initial condition run with different feedback agents, we are able to underpin the effects of these agents within the mass range of $\sim 10^9 - 10^{11}\, M_\odot$. Hence, the analysis should be taken on individual galaxy basis, and as a first step toward understanding the impact of BHXs as a possible feedback mechanism.

We carry out an analysis of the simulated galaxies from $z \sim 9$ to $z \sim 4$. For each available snapshot of the simulations, simulated galaxies are defined at the optical radius which corresponds to that enclosing 83% of the baryonic mass of the selected system. The dark matter halo masses are calculated at the virial radius.

4.1 The stellar-to-dark mass ratio

First, we study the ratio between the mean stellar mass and their virial halo mass of the simulated galaxies as a function of the latter. The estimated relations for S230-SN and S230-BHX are shown in Fig. 3. For comparison, we also show the results obtained using the abundance matching technique by Behroozi et al. (2013) at redshift $z \sim 7, 5, 4$, and by Moster et al. (2013) at redshift $z \sim 4$. In the case of Moster et al. (2013) data, we extrapolate their stellar-to-halo mass relation to lower halo masses. We note that the simulations tend to resolve smaller virial haloes compared to those shown by Behroozi et al. (2013), except for $z \sim 7$ where there is a better match of the mass range. Therefore, we extrapolate the trends to draw conclusions.

---

[2] The impact of BHX feedback on the global SF activity when the numerical resolution is increased is similar, although as explained before, S320 runs formed more stars for the same set of SN and SF parameters (see Section 2.1.1). By comparing the energy released by BHX and SNII events in S320-SN and S320-BHX, we found a maximum of $\sim$ 30% contribution from BHX feedback, that decays rapidly with redshift as the ISMs are chemically enriched, in a similar fashion as reported for S230 in Section 3. The specific redshift at which BHX feedback is maximum over SNII feedback is a statement which depends on the box-size. Our simulated box correspond to a small field region, so a larger volume will be required to make a full statement on this aspect.

At $z \sim 7$, there is an excess of stars in small haloes in S230-SN compared to those detected in S230-BHX. This excess originates in the very efficient transformation of gas into stars at the early stages of evolution in S230-SN as also reported in previous works (e.g. Sawala et al. 2011; De Rossi et al. 2013). Although our SN feedback model is successful at producing galactic outflows and fountains, which regulate the star formation, it is less efficient in the first stages of galaxy formation. When the energy released by BHXs is added to the SN feedback, then a decrease in the star formation activity at high redshift is detected. In Fig. 2, we compared the relative importance of both feedback mechanisms as a function of redshift. In Fig. 3 we can appreciate the effects on individual galaxies. In fact, the regulation of the star formation by BHX events is more efficient in low mass haloes, steepening the relation between the stellar-to-halo mass ratio and the halo mass of the galaxies. In haloes less massive than $\sim 10^{10}\,M_{\odot}$, simulated galaxies in S230-BHX have less stellar mass than those in S230-SN. For larger halo masses instead, the simulated galaxies in S230-BHX reach larger fractions of stars compared to the SN feedback run. This trend is produced because simulated galaxies in these haloes have larger amount of gas to feed the subsequent star formation process. This can be explained as a consequence of the impact of BHXs at early times, when the systems were smaller and could be affected by BHX feedback.

We note that although the cSFR of S230-BHX reproduces the observations compiled by Behroozi et al. (2013), there seems to be still more stars per dark matter halo at $z \lesssim 7$. However, the slope of stellar-to-halo mass relation agrees better to the extrapolation of observations for lower masses. This is also valid when compared to Moster et al. (2013) at $z \sim 4$.

4.2 Gas fractions

The impact of the SN and BHX feedback on the stellar mass of galaxies can be also studied by comparing the ratio between the mean gas mass and the virial halo mass. Fig. 4 shows this relation as a function of the halo mass for galaxies in S230-BHX and S230-SN, and for the same redshift range displayed in Fig. 3. The gas mass of the simulated galaxies is estimated as the total mass of gas particles inside their optical radii.

As can be seen from Fig. 4, simulated galaxies in S230-BHX have higher gas masses than those in the simulation without BHX feedback, regardless of their host haloes. At $z \sim 7$, we detect the smaller gas fraction in S230-SN for $M_{\rm h} > 10^{10}\,M_{\odot}$. This result seems to be at odds with the trends shown in Fig. 3, under the hypothesis of a close-box model. Indeed, if there were no gas infall or outflow, then the galaxies with the larger stellar mass fraction should have had the smaller gas fraction. However, this is not what we see in Fig. 4. The fact that galaxies in S230-BHX have larger fraction of gas within their optical radii suggests that their counterparts in S230-SN have lost larger fractions of their gas reservoirs and hence, the subsequent star formation is lower. If this were the case, then galactic outflows should have carried out more material to the circumgalactic medium (CGM) of these galaxies, increasing its temperature.

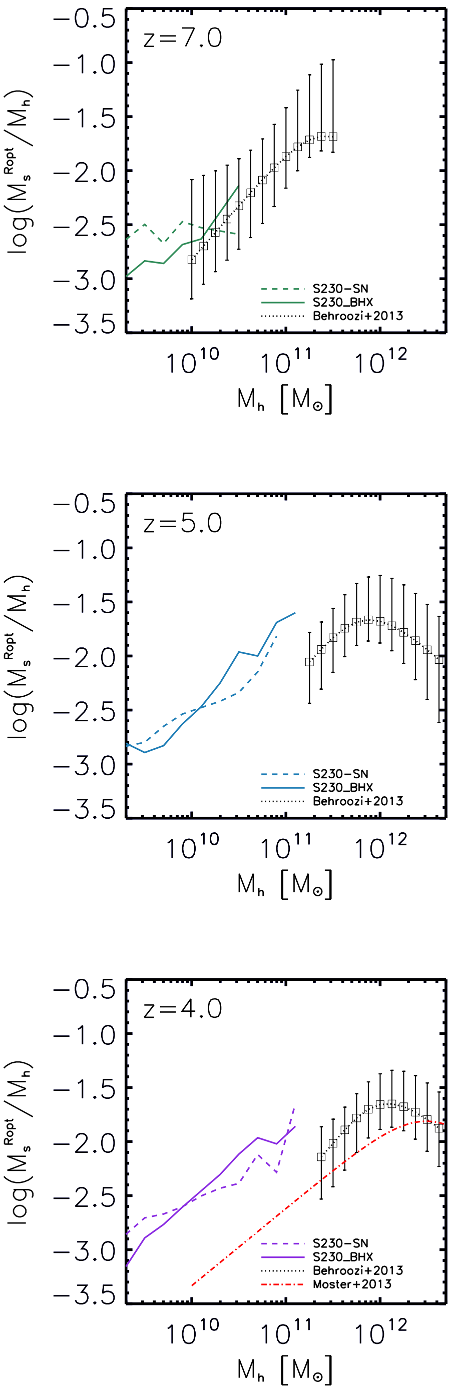

Figure 3. Mean stellar-to-halo mass ratio as a function of halo mass, for redshifts $z \sim 7$, 5 and 4. We estimate the stellar mass of a galaxy as the total mass of stellar particles inside the optical radius. Dashed lines represent galaxies in S230-SN, while solid lines show those in S230-BHX. The results of abundance matching techniques taken from Behroozi et al. (2013) are plotted in black as open squares plus a dotted line. For $z \sim 4$ we include also the extrapolation of the data of Moster et al. (2013) (dash-dotted red line).

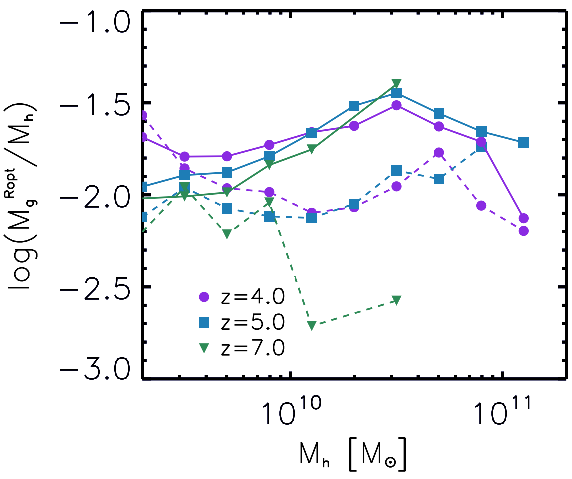

Figure 4. Gas-to-halo mass ratio as a function of halo mass for simulated galaxies in S230-BHX (solid lines) and S230-SN (dashed lines). The relations are shown for three different redshifts: $z = 7$ (green triangles), 5 (blue squares), and 4 (violet circles). Gas mass is estimated as the total mass of gas particles enclosed within the optical radius of a galaxy at a given redshift.

In order to analyse this feedback loop between the ISM and the CGM of the simulated galaxies, we estimate the fraction of the total gas mass within the virial radius which remains within the optical radius in both simulations. As can be seen in Fig. 5, in S230-BHX, simulated galaxies in haloes with virial masses in the range $10^{10}\, M_\odot \lesssim M_\mathrm{h} \lesssim 10^{11}\, M_\odot$ are able to retain larger amounts of gas than their counterparts in S230-SN. For smaller and larger haloes, both simulations show the same level of remnant gas within the optical radius. In the quoted halo-mass range, galaxies in S230-SN have been able to loose a larger fraction of gas, which can be understood considering their higher early star-formation activity. As a consequence, gas outflows are triggered, expelling larger amount of gas. This produces a decrease of the star formation activity afterwards since there is less gas to fuel it. In fact, as shown in Fig. 1, the star formation activity of S230-SN at low redshift remains lower than that estimated by Behroozi et al. (2013), whereas it is higher at high redshift. Hence, this suggests that it will not be possible to reach an agreement if only SN feedback is present (see also Stinson et al. 2012). Increasing the SN feedback to decrease the star formation at high redshift would make the discrepancy at lower redshift even larger. It is the action of the BHX feedback that helps to regulate the star formation at very high redshifts, which then results in the desired trend at lower ones.

As we can see from Fig. 3, there seems to be a halo mass threshold below which BHXs are efficient at modulating the star formation. This is approximately $M_\mathrm{h} \sim 10^{10}\, M_\odot$, which corresponds to circular velocities $V_\mathrm{vir} \sim 40\,\mathrm{km\,s^{-1}}$ or a virial temperature of $T_\mathrm{vir} \sim 50,000\,\mathrm{K}$ (assuming primordial abundances). For galaxies below this threshold, the BHX feedback is strong enough to heat the ISM to $T \sim T_\mathrm{vir}$, decreasing the star formation activity without expelling a significant fraction of gas mass.

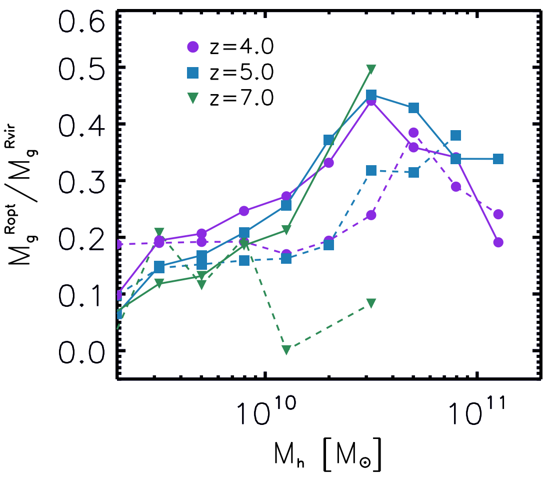

Figure 5. Fraction of the total gas within the virial radius retained within the optical radius, for simulated galaxies in S230-BHX (solid lines) and in S230-SN (dashed lines) at $z = 7$ (green triangles), 5 (blue squares), and 4 (violet circles).

To illustrate this, in Fig. 6 we show the mean temperature of the gas within the optical (left panels) and the virial (right panels) radius, for simulated galaxies in both runs, at $z \sim 7$ and $z \sim 5$. The run with BHXs shows hotter environment within the optical radius, although with temperatures smaller than T_vir. Conversely, galaxies in S230-SN have lost gas by SN feedback. In fact, SN feedback has been successful at building a hot CGM even at these high redshifts. The CGMs are colder in the run with S230-BHX, since the total stellar mass formed per halo is not enough to drive powerful winds yet. The BHX feedback has contributed to heat up the gas within the galaxies, decreasing the mass of new-born stars in haloes with $M_\mathrm{h} < 10^{10}\, M_\odot$. Therefore, as they grow by hierarchical clustering, they will be able to have larger gas reservoirs to continue their star formation activity. Later on, as the SN rate increases, the SN feedback contributes to heat up the CGM of galaxies in S230-BHX.

4.3 The stellar mass of galaxies

To assess how the effects of BHX feedback modifies the stellar mass of galaxies, we estimate the cumulative number of galaxies as a function of their stellar mass. As it can be seen from Fig. 7, the simulations behave differently. The simulation with BHX feedback shows a notable evolution with redshift, with $\sim 80\%$ of the galaxies exhibiting stellar masses smaller than $10^7\, M_\odot$ at $z \sim 7$, percentage which decreases to $\sim 50\%$ at $z \sim 4$. Conversely, the simulation with only SN feedback does not present a clear evolution in this redshift range. On average, $\sim 50-60\%$ of the galaxies have stellar masses smaller than $\sim 10^7\, M_\odot$. These trends confirm that galaxies in S230-BHX form less stars in small galaxies than those in S230-SN. Hence, BHX thermal feedback affects directly small galaxies but indirectly larger ones. Those mostly affected have stellar masses between 10^7 and $10^8\, M_\odot$ and inhabit haloes with $V_\mathrm{vir} \sim 40$ km s^{-1}.

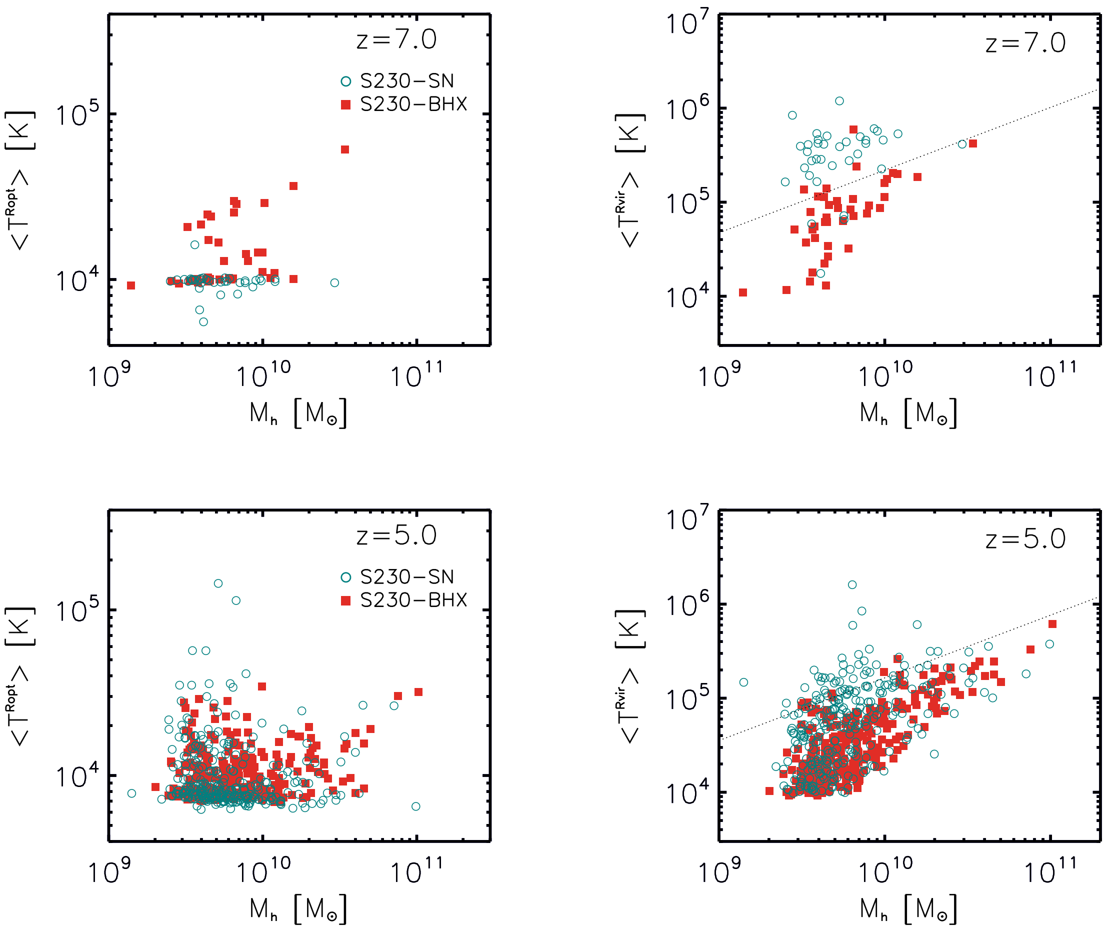

Figure 6. Median temperatures of the gas component within the optical radius (left panels) and within the virial radius (right panels), for galaxies in S230-BHX and S230-SN at $z = 7$ and $z = 5$. The dotted lines represent the relation between virial mass and virial temperature. Note that at $z = 7$, simulated galaxies in S230-BHX have hotter interstellar media than their counterparts in S230-SN. Conversely, the circumgalactic media of galaxies in S230-SN get hotter sooner, as a consequence of the hot material transported by outflows. These outflows are triggered by the more violent SN feedback, produced by the larger SFR taken place in this run at very high redshift.

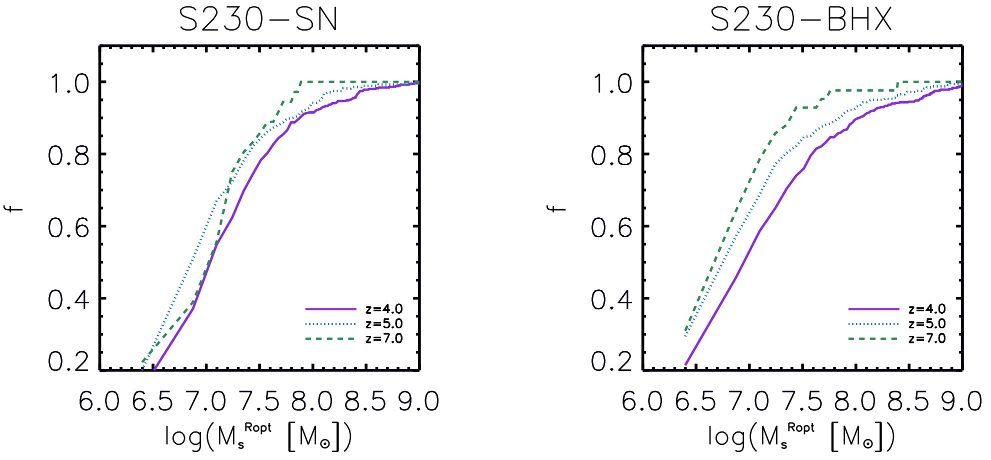

Figure 7. Cumulative distribution of the stellar mass within the optical radius at $z \sim 7$ (green dashed line), $z \sim 5$ (blue dotted line) and $z \sim 4$ (violet solid line). *Left:* Simulation without BHX feedback. *Right:* Simulation with BHX feedback.

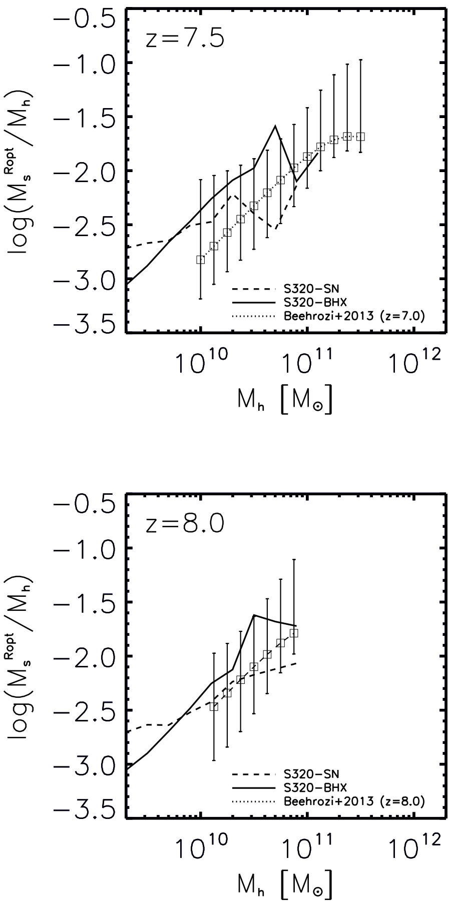

Figure 8. Mean stellar-to-virial mass relation at $z = 7$ and $z = 8$, for simulated galaxies in S320-SN (dashed lines) and S320-BHX (solid lines). The results of abundance matching technique from Behroozi et al. (2013) are included (dotted line plus empty squares). The main impact of BHX feedback occurs for $M_{\rm h} < 10^{10}\,M_\odot$, in agreement with results found for S230-BHX.

4.4 Testing numerical resolution

In order to test the robustness of our trends against numerical resolution, we analyse the simulated galaxies in S320-SN and S320-BHX at $z \sim 7.5$ and $z \sim 8$. Galaxies have been selected and analysed by using the same criteria, although the minimum number of particles was increased to 2000 in order to avoid including very small systems which were not considered in S230-BHX.

In Fig. 8 we show the stellar-to-virial mass relation in a similar fashion as in Fig. 3. The relations for galaxies in S320-BHX and S320-SN cross each other at about $M_{\rm h} \sim 10^{10}\,M_\odot$ in agreement with the trends found in the S230 runs. Even more, the cumulative distribution of stellar mass also exhibits a similar trend to those found in S230 (Fig. 7). And as a consequence, this agreement between the low and high resolution runs suggest that the results are numerically robust.

4.5 Contribution of X-ray photons

As already discussed, the rate and X-ray luminosity of BHXs are expected to be highly related to the metallicity of the progenitor stars as suggested by observational and theoretical studies. Due to the long-mean free path of X-ray photons, BHXs could contribute significantly to the heating and ionization of the IGM at early stages of galaxy evolution (e.g. Mirabel et al. 2011; Jeon et al. 2014; Power et al. 2013; Knevitt et al. 2014). Mirabel et al. (2011) show how the evolution of the temperature of the low-density neutral IGM due to heating by X-rays from BHXs may depend on the value of the parameter $f_{\rm X}$. This parameter is defined as the ratio of the total X-ray luminosity $L_{\rm X}$ of a galaxy in the 2–10 keV band to its SFR, and its value can be estimated from the expression

$$f_{\rm X} = (3.5 \times 10^{40}\,{\rm SFR})^{-1} L_{\rm X}, \qquad (1)$$

where $L_{\rm X}$ is measured in ${\rm erg\,s^{-1}}$ and the SFR in $M_\odot\,{\rm yr}^{-1}$. An increase of $f_{\rm X}$ would cause the neutral IGM to be heated earlier due to the presence of BHXs. This could limit the cold gas accretion in dwarf galaxies at high redshift.

Although the detailed analysis of X-ray feedback of BHXs into the IGM is out of the scope of this work, we estimate the value of $f_{\rm X}$ using our model for extremely metal-poor BHXs in order to evaluate its compatibility with expectations from other models. The emission of these BHXs should dominate the X-ray luminosity of star-forming galaxies mainly at high redshift when most young stellar populations were metal-poor. In any case, our predicted $f_{\rm X}$ represents a lower limit, resulting in a conservative contribution to radiative feedback in the early Universe.

Assuming that BHXs radiate a similar amount of energy in X-ray luminosity to that injected in kinematic outflows (i.e. $\epsilon_{\rm X} = E_{\rm BHX} = 10^{52}\,{\rm erg}$), and a mean emission time of ~ 3 Myr, the mean X-ray luminosity per source as $L_{\rm X} \sim 10^{38}\,{\rm erg\,s^{-1}}$, as already mentioned in Section 2.2. If the number of BHXs produced in a galaxy is $N_{\rm BHX}$, then the mean total X-ray luminosity of a simulated galaxy originated from BHXs is $L_{\rm X}^{\rm G} = N_{\rm BHX} L_{\rm X}$, which can be easily computed at each time step of the simulation. To make a proper comparison with Mirabel et al. (2011), we use the galaxy catalogue of S320-BHX at $z \sim 9$. These simulated galaxies have SFR and $L_{\rm X}^{\rm G}$ in the range $[0.01 - 20]\,M_\odot{\rm yr}^{-1}$ and $[10^{39} - 10^{41}]{\rm erg\,s^{-1}}$, respectively. Hence, the mean $f_{\rm X}$ value obtained at $z \sim 9$ is $\langle f_{\rm X} \rangle = 0.65$.

Note that the total X-ray luminosities of simulated galaxies do not exceed the X-ray luminosity limit of the deepest surveys (4 Ms Chandra Deep Field-South —CDF-S—, Xue et al. 2011). At $z \sim 9$, the 2–10 keV rest frame energy band corresponds roughly to the observed soft band 0.2–1 keV. The flux limit of the 4 Ms CDF-S in the soft band is $9.1 \times 10^{-18}{\rm erg\,cm^{-2}\,s^{-1}}$, therefore the (k-corrected) luminosity limit at $z \sim 9$ is $L_{\rm X,lim} \sim 4.6 \times 10^{42}\,{\rm erg\,s^{-1}}$. Hence, our BHXs model does not contradict the upper limits imposed by current surveys.

The $\langle f_{\rm X} \rangle$ value obtained does not take into account the absorption of X-ray photons before reaching the IGM. A rough estimation of the fraction of escaping photons into the IGM could be obtained by adopting a power law spectral energy distribution for the sources, with an index of 1.7 in the 0.5–10 keV range (Swartz et al. 2004). We calculate this fraction for a typical halo of $M_{\rm h} = 10^8\,M_\odot$, assuming an exponential surface density for the galaxy. We assume that the ratio of the baryonic-to-dark-matter mass is $m_{\rm d} = 0.17$, the spin parameter is $\lambda \sim 0.03$ and $j_{\rm d}/m_{\rm d} = 1$, where $j_{\rm d}$ is the ratio of the angular momentum of baryons to that of the halo (Mo et al. 1998; Fernandez & Shull 2011). Considering that X-ray photons would ionize both hydrogen and helium in the IGM, we use the cross sections of Kuhlen & Madau (2005). The estimated escape fraction is then $f_{\rm esc} \sim 0.53$. Therefore, the effective $\langle f_{\rm X}\rangle$ would be $\langle f_{\rm X}\rangle_{\rm eff} \sim 0.34$ at redshift $z \sim 9$. This value is lower than that proposed by Mirabel et al. (2011) where $f_{\rm esc} \sim 1.0$ is assumed. Our simple estimation implies that the generated X-ray photons could barely heat the temperature of the IGM above 10^3 K. However, our estimations are too crude to draw more robust conclusions on this aspect. This effect can be studied with radiative transfer models in detail (e.g. Knevitt et al. 2014).

5 CONCLUSIONS

In this work, we explore the effects of HMXBs composed by an accreting black hole on galaxy evolution (Justham & Schawinski 2012). Following previous results, our model assumes that the rate, X-ray luminosity and outflow energy of BHXs increase for low metallicity progenitors (Dray 2006; Linden et al. 2010). The BHX feedback model is grafted into a version of P-GADGET-3 which includes SN feedback and chemical evolution (Scannapieco et al. 2006), so that its effects can be studied as the structure forms and evolves.

The estimated kinetic energy released by BHXs is assumed to be efficiently thermalized and hence, is pumped into the cold gaseous phase in the surrounding region of the sources. This extra source of energy has an impact on the properties of the ISM at early stages of evolution and in low-velocity haloes. Encouragingly, our results agree with those reported by (Justham & Schawinski 2012) where a semi-analytical model was used to implement a scheme based on similar hypotheses.

Our results can be summarized as follows:

- Following observations which indicate that the kinetic energy deposited by these sources might be comparable to that radiated in the X-ray bands (during ~ 3 Myr), we estimate that each BHX event could inject $\sim 10^{52}$ erg in form of kinetic energy in the ISM. With these hypotheses and in order to reproduce the observed cSFR, our BHX model requires that a fraction of $\sim 20\%$ of BHs with metallicity in the range $Z_{\rm EMP} = [0, 10^{-4}]$ should end up as X-ray binary systems. We tested combinations of larger and lower released kinetic energy and BHX fractions finding that they produce too strong or too weak effects, resulting in an inadequate regulation of the star formation at high redshift.
- Our model predicts BHX feedback to affect more strongly galaxies with stellar masses in the range 10^7–$10^8\,M_\odot$ which inhabit haloes with virial velocities smaller than $V_{\rm vir} \sim 40\,{\rm km\,s^{-1}}$. Larger haloes would experience a negligible impact due to their larger potential wells but they could be indirectly affected by the accretion of smaller haloes. These results are shown to be robust against numerical resolution.
- The energy injected by BHXs helps to regulate the star formation activity in low-mass haloes, decreasing the fraction of stars formed at very high redshift. As a consequence, there is more gas available for star formation at later times. Therefore, when BHX feedback is included, the cSFR reproduces closely observational results (Behroozi et al. 2013). In this simulated volume, we found the BHX energy represents a $\sim 30\%$ of total feedback energy released into the ISM at $z \sim 7$, and a 10% at $z \sim 4$.
- When BHX feedback is included the number of galaxies as a function of stellar masses shows a larger evolution with redshift (for $z > 4$) compared to the run with only SN feedback turned on. The variation of the evolution is driven by the low-mass haloes which are more significantly affected by BHX feedback, and hence, its characteristics could be an observational test to probe the action of this feedback.
- The stellar-to-virial mass relation for $z \sim 7$ is in better agreement to that predicted from abundance matching (Moster et al. 2013; Behroozi et al. 2013). For lower redshift, there is still an excess of stars, although the slope of the relation is more comparable to the predicted trends.
- Simulated galaxies with BHX+SN feedbacks exhibit hot ISM at very high redshift but their mean temperature is smaller than the virial temperature of the haloes. If the BHX feedback is switched off, the resulting ISM are colder and the fraction of new born stars higher in low mass haloes. As a consequence the number of SNe is enough to blow part of the ISMs, contributing to building up hotter CGMs. In order to prevent this, the SN feedback should be weaken but this would lead to a further increase of the star formation, producing a larger stellar fraction.

Hence, our results support previous claims that the BHXs could be an important source of feedback in early stages of galaxy evolution by regulating the star formation in haloes with $V_{\rm vir} \leqslant 40\,{\rm km\,s^{-1}}$. It goes in the same direction as the so-called 'enhanced' feedback although BHX feedback would have significant impact only in the very early Universe.

ACKNOWLEDGEMENTS

We would like to thank the referee, Dr Graham Wynn, for his careful reading and comments which helped to improve the paper, and Laura Sales for useful discussions. Simulations are part of the Fenix Project and have been run in Hal Cluster of the Universidad Nacional de Córdoba, AlphaCrucis of IAG-USP (Brasil) and Barcelona Supercomputer Center. We acknowledged the use of Fenix Cluster of Institute for Astronomy and Space Physics. This work has been partially supported by PICT Raices 2011/959 of Ministery of Science (Argentina) and Proyecto Interno of Universidad Andres Bello (Chile).

REFERENCES

Behroozi P. S., Wechsler R. H., Conroy C., 2013, ApJ, 770, 57

Belczynski K., Sadowski A., Rasio F. A., 2004, ApJ, 611, 1068

Brorby M., Kaaret P., Prestwich A., 2014, MNRAS, 441, 2346

Ceverino D., Klypin A., Klimek E. S., Trujillo-Gomez S., Churchill C. W., Primack J., Dekel A., 2014, MNRAS, 442, 1545

Chabrier G., 2003, PASP, 115, 763

Chen K.-J., Bromm V., Heger A., Jeon M., Woosley S., 2014, ArXiv e-prints

De Rossi M. E., Avila-Reese V., Tissera P. B., González-Samaniego A., Pedrosa S. E., 2013, MNRAS, 435, 2736

Dekel A., Silk J., 1986, ApJ, 303, 39

Dray L. M., 2006, MNRAS, 370, 2079

Fabbiano G., 2006, ARA&A, 44, 323

Fender R. P., Maccarone T. J., van Kesteren Z., 2005, MNRAS, 360, 1085

Feng H., Soria R., 2011, New Astronomy Reviews, 55, 166

Fernandez E. R., Shull J. M., 2011, ApJ, 731, 20

Fialkov A., Barkana R., Visbal E., 2014, Nature, 506, 197

Fragos T., Lehmer B., Tremmel M., Tzanavaris P., Basu-Zych A., Belczynski K., Hornschemeier A., Jenkins L., Kalogera V., Ptak A., Zezas A., 2013, ApJ, 764, 41

Fragos T., Lehmer B. D., Naoz S., Zezas A., Basu-Zych A., 2013, ApJ, 776, L31

Gallo E., Fender R., Kaiser C., Russell D., Morganti R., Oosterloo T., Heinz S., 2005, Nature, 436, 819

Georgy C., Meynet G., Walder R., Folini D., Maeder A., 2009, A&A, 502, 611

Governato F., Willman B., Mayer L., Brooks A., Stinson G., Valenzuela O., Wadsley J., Quinn T., 2007, MNRAS, 374, 1479

Hopkins P. F., Kereš D., Oñorbe J., Faucher-Giguère C.-A., Quataert E., Murray N., Bullock J. S., 2014, MNRAS, 445, 581

Iwamoto K., Brachwitz F., Nomoto K., Kishimoto N., Umeda H., Hix W. R., Thielemann F.-K., 1999, ApJS, 125, 439

Jeon M., Pawlik A. H., Bromm V., Milosavljević M., 2014, MNRAS, 440, 3778

Jimenez N., Tissera P. B., Matteucci F., 2014, ArXiv e-prints

Justham S., Schawinski K., 2012, MNRAS, 423, 1641

Kaaret P., 2014, MNRAS, 440, L26

Kaaret P., Schmitt J., Gorski M., 2011, ApJ, 741, 10

Knevitt G., Wynn G. A., Power C., Bolton J. S., 2014, MNRAS, 445, 2034

Kuhlen M., Madau P., 2005, MNRAS, 363, 1069

Linden T., Kalogera V., Sepinsky J. F., Prestwich A., Zezas A., Gallagher J. S., 2010, ApJ, 725, 1984

Mirabel I. F., Dijkstra M., Laurent P., Loeb A., Pritchard J. R., 2011, A&A, 528, A149

Mo H. J., Mao S., White S. D. M., 1998, MNRAS, 295, 319

Mosconi M. B., Tissera P. B., Lambas D. G., Cora S. A., 2001, MNRAS, 325, 34

Moster B. P., Naab T., White S. D. M., 2013, MNRAS, 428, 3121

Pacucci F., Mesinger A., Mineo S., Ferrara A., 2014, MNRAS, 443, 678

Pakull M. W., Mirioni L., 2003, in Arthur J., Henney W. J., eds, Revista Mexicana de Astronomia y Astrofisica Conference Series Vol. 15 of Revista Mexicana de Astronomia y Astrofisica Conference Series, Bubble Nebulae around Ultraluminous X-Ray Sources. pp 197–199

Pakull M. W., Soria R., Motch C., 2010, Nature, 466, 209

Pedrosa S. E., Tissera P. B., De Rossi M. E., 2014, A&A, 567, A47

Power C., James G., Combet C., Wynn G., 2013, ApJ, 764, 76

Power C., Wynn G. A., Combet C., Wilkinson M. I., 2009, MNRAS, 395, 1146

Ramsey C. J., Williams R. M., Gruendl R. A., Chen C.-H. R., Chu Y.-H., Wang Q. D., 2006, ApJ, 641, 241

Sawala T., Guo Q., Scannapieco C., Jenkins A., White S., 2011, MNRAS, 413, 659

Scannapieco C., Tissera P. B., White S. D. M., Springel V., 2005, MNRAS, 364, 552

Scannapieco C., Tissera P. B., White S. D. M., Springel V., 2006, MNRAS, 371, 1125

Scannapieco C., Tissera P. B., White S. D. M., Springel V., 2008, MNRAS, 389, 1137

Scannapieco C., White S. D. M., Springel V., Tissera P. B., 2009, MNRAS, 396, 696

Soria R., Long K. S., Blair W. P., Godfrey L., Kuntz K. D., Lenc E., Stockdale C., Winkler P. F., 2014, Science, 343, 1330

Soria R., Pakull M. W., Broderick J. W., Corbel S., Motch C., 2010, MNRAS, 409, 541

Springel V., 2005, MNRAS, 364, 1105

Springel V., Frenk C. S., White S. D. M., 2006, Nature, 440, 1137

Springel V., White S. D. M., Tormen G., Kauffmann G., 2001, MNRAS, 328, 726

Stinson G. S., Brook C., Prochaska J. X., Hennawi J., Shen S., Wadsley J., Pontzen A., Couchman H. M. P., Quinn T., Macciò A. V., Gibson B. K., 2012, MNRAS, 425, 1270

Sutherland R. S., Dopita M. A., 1993, ApJS, 88, 253

Swartz D. A., Ghosh K. K., Tennant A. F., Wu K., 2004, ApJS, 154, 519

Wadepuhl M., Springel V., 2011, MNRAS, 410, 1975

Woosley S. E., Weaver T. A., 1995, ApJS, 101, 181

Xue Y. Q., Luo B., Brandt W. N., Bauer F. E., Lehmer B. D., Broos P. S., Schneider D. P., Alexander D. M., Brusa M., Comastri e. a., 2011, ApJS, 195, 10